

Article

Clarification of Active Sites at Interfaces between Silica Support and Nickel Active Components for Carbon Monoxide Methanation

Mengjuan Zhang ^{1,†}, Panpan Li ^{1,†}, Zhiqun Tian ², Mingyuan Zhu ¹, Fu Wang ³, Jiangbing Li ¹, Bin Dai ¹, Feng Yu ^{1,*} , Hengshan Qiu ^{3,*}  and Hongwei Gao ^{4,*}

¹ Key Laboratory for Green Processing of Chemical Engineering of Xinjiang Bingtuan, School of Chemistry and Chemical Engineering, Shihezi University, Shihezi 832003, China; mengjuanzhang2017@126.com (M.Z.); ppl_19910109@163.com (P.L.); zhumin yuan@shzu.edu.cn (M.Z.); ljbing@126.com (J.L.); db_tea@shzu.edu.cn (B.D.)

² Collaborative Innovation Center of Renewable Energy Materials, Guangxi University, Nanning 530004, China; tianzhiqun@gxu.edu.cn

³ Xinjiang Technical Institute of Physics and Chemistry, Chinese Academy of Sciences, Urumqi 830011, China; wangfu@ms.xjb.ac.cn

⁴ School of Life Science, Ludong University, Yantai 264025, China

* Correspondence: yufeng05@mail.ipc.ac.cn (F.Y.); qiu@ms.xjb.ac.cn (H.Q.); gaohongw369@163.com (H.G.); Tel.: +86-993-205-7272 (F.Y.); +86-991-369-0837 (H.Q.); +86-535-668-5003 (H.G.); Fax.: +86-993-205-7270 (F.Y.); +86-991-369-0837 (H.Q.); +86-535-668-5003 (H.G.)

† These authors contributed equally to this work.

Received: 13 June 2018; Accepted: 16 July 2018; Published: 20 July 2018



Abstract: Identification of active site is critical for developing advanced heterogeneous catalysis. Here, a nickel/silica (Ni/SiO₂) catalyst was prepared through an ammonia-evaporation method for CO methanation. The as-obtained Ni/SiO₂ catalyst shows a CO conversion of 96.74% and a methane selectivity of 93.58% at 623 K with a weight hourly space velocity of 25,000 mL·g⁻¹·h⁻¹. After 150 h of continuous testing, the CO conversion still retains 96%, which indicates a high catalyst stability and long life. An in situ vacuum transmission infrared spectrum demonstrates that the main active sites locate at the interface between the metal Ni and the SiO₂ at a wave number at 2060 cm⁻¹ for the first time. The interesting discovery of the active site may offer a new insight for design and synthesis of methanation catalysts.

Keywords: active sites; carbon monoxide methanation; ammonia-evaporation method; in situ vacuum transmission infrared spectroscopy; density-functional theory

1. Introduction

With the increasing global demand for clean energy sources, natural gas, the main ingredient of methane (CH₄), is promising as a clean energy source, which replaces conventional fossil fuels that have resulted in a range of environmental issues [1,2]. Carbon monoxide (CO) methanation is an ideal way to produce CH₄ from coal, and has proven to be one of the most effective ways for the clean utilization of coal [3,4]. Previous research has focused on improving the required catalytic performance of nickel-based catalysts in CO methanation [5–7]. Especially, nickel/silica (Ni/SiO₂) catalyst attracted significant attention due to its high efficient activity for CO methanation [8,9].

Enlarged active sites of Ni/SiO₂ are significant routes to enhance activity of CO catalytically converted to synthetic natural gas (SNG) for clean energy in C1 Chemistry [4]. Generally, a smaller Ni particle size gives a better performance and provides the important route of strengthen the

activity of CO methanation. Yan et al. [10] and Zhao et al. [11] found that a smaller Ni particle size, a higher Ni particles dispersion and an enhanced interaction between Ni and the SiO₂ support via dielectric-barrier discharge (DBD) plasma decomposition method exhibited significantly improved activity with enhanced stability. Li et al. [12] reported a superior position for implantation of Ni species on two-dimensional porous SiO₂ nanomesh rather than three-dimensional MCM-41, resulting in high Ni dispersion and activity.

Despite numerous studies on the use of smaller Ni particles to improve the catalytic performance, little comprehensive understanding exists of the microscopic mechanism. Yao et al. [13] studied Cu–Ni/SiO₂ catalysts via in situ CO polarization modulation infrared reflection absorption spectroscopy (PM-IRRAS) and found that CO-induced surface segregation of Ni easily resulted in severe errors in Ni active site measurements via the selective CO chemisorption. Loc et al. [14] measured kinetic isotope effects on Ni-based catalysts via the replacement of hydrogen by deuterium in CO methanation and found that interaction of oxygen-containing compounds with hydrogen was a slow step of the process. Martra et al. [15] reported that the high Ni dispersion provided good CO adsorption on metal-support interaction via in situ diffuse reflectance Fourier transform infrared spectroscopy (DRIFTS). Primet et al. [16] studied CO adsorption on Ni/SiO₂ catalysts via infrared spectroscopy and saturation magnetization and found that the presence of two bands in the region corresponding to linear species (2070 and 2040 cm^{−1}) with intensities ratios varying with the degree of NiO reduction. These concerns, along with essential demands to incorporate activity for CO methanation, led scientists towards the study of active sites.

Herein, we have prepared an Ni/SiO₂ catalyst by the ammonia-evaporation (AE) method, and have explored the active sites for CO methanation by in situ vacuum transmission infrared (VTIR) spectroscopy and density-functional theory (DFT) calculations. The in situ VTIR results indicated that the main active site was the interface between the metal Ni and silica (SiO₂) support. DFT was used to confirm the CO adsorption behavior in various types of adsorption sites. We believe that clarifications of active sites at the interface between silica support and nickel active component afford an effective way to design and prepare a high-efficiency CO methanation catalyst.

2. Results and Discussion

2.1. Schematic Illustration

In order to explore the reaction mechanism of the CO methanation by Ni-based catalysts, our main design was to combine the actual value with the theoretical calculated value to speculate the bonded sites of CO species. First, from the results of in situ Fourier Transform infrared spectroscopy (FTIR) spectra, we found there were four types of adsorption sites: the NiO or SiO₂ surface, the top Ni atom surface, the interface between the SiO₂ and Ni atom, and the bridge of the surface Ni atoms. Combined with the results of in situ FTIR differential spectra of catalyst Ni/SiO₂ at 500 K in the presence of CO and H₂ at different reaction times, an obvious negative peak at 2060 cm^{−1} suggesting an interface between SiO₂ and Ni, which means that the interface between the SiO₂ and Ni atoms played a key role in the CO methanation reaction. The interface adsorption has two main types: Ni–SiO₂ and Ni–O. From the results of DFT, the theoretical value of Ni–SiO₂ and Ni–O interface adsorption presented at 1859 cm^{−1} and 2019 cm^{−1}, respectively. It indicated that the Ni–O interface adsorption was the main point adsorption site and the red-shift about the vibration peak was due to the synergistic effect of Ni–SiO₂ interface adsorption.

2.2. Catalytic Performance

A previous study indicated that smaller Ni particles provide a better catalytic performance, with a higher CO conversion and CH₄ selectivity [17]. The catalytic performance of Ni/SiO₂ was tested at the range of 523–823 K, 1.5 MPa, with a weight hourly space velocity (WHSV) of 25,000 mL·g^{−1}·h^{−1}. Before the test, only a small part of the NiO on the catalyst was reduced to Ni, and low Ni loading and

high Ni dispersion provided efficient active sites [18]. The Ni/SiO₂ catalyst displayed an excellent catalytic performance over the entire reaction temperature.

As shown in Figure 1a, the catalyst displayed a 91.7% CO conversion at 523 K, and achieved a maximum CO conversion at 623 K with a CO conversion of 96.7%. The CO conversion decreased with temperature, and showed an 89.0% CO conversion at 823 K. The CH₄ selectivity of the Ni/SiO₂ catalyst showed the same tendency with CO conversion, and achieved a maximum CH₄ selectivity of 95.6% at 623 K. The turnover frequency (TOF) values were calculated by Ni dispersion which were obtained by hydrogen adsorption method. It showed that TOF increased with an increasing temperature, and achieved a maximum value of 17.6 s⁻¹ at 623 K, then decreased with rising temperatures, and showed an 89.0% CO conversion and 16.2 s⁻¹ TOF at 823 K. The as-obtained catalyst maintained efficient catalytic activity for 150 h at 623 K, 1.5 MPa with a WHSV of 25,000 mL·g⁻¹·h⁻¹. Figure 1b shows only a 3% decreased CO conversion, which indicated that the Ni/SiO₂ catalyst presented an excellent thermodynamic stability. Besides, the Ni/SiO₂ catalyst by AE method showed strong interactions between Ni and the silica support, which promoted the formation of a stable structure and prevented Ni aggregation.

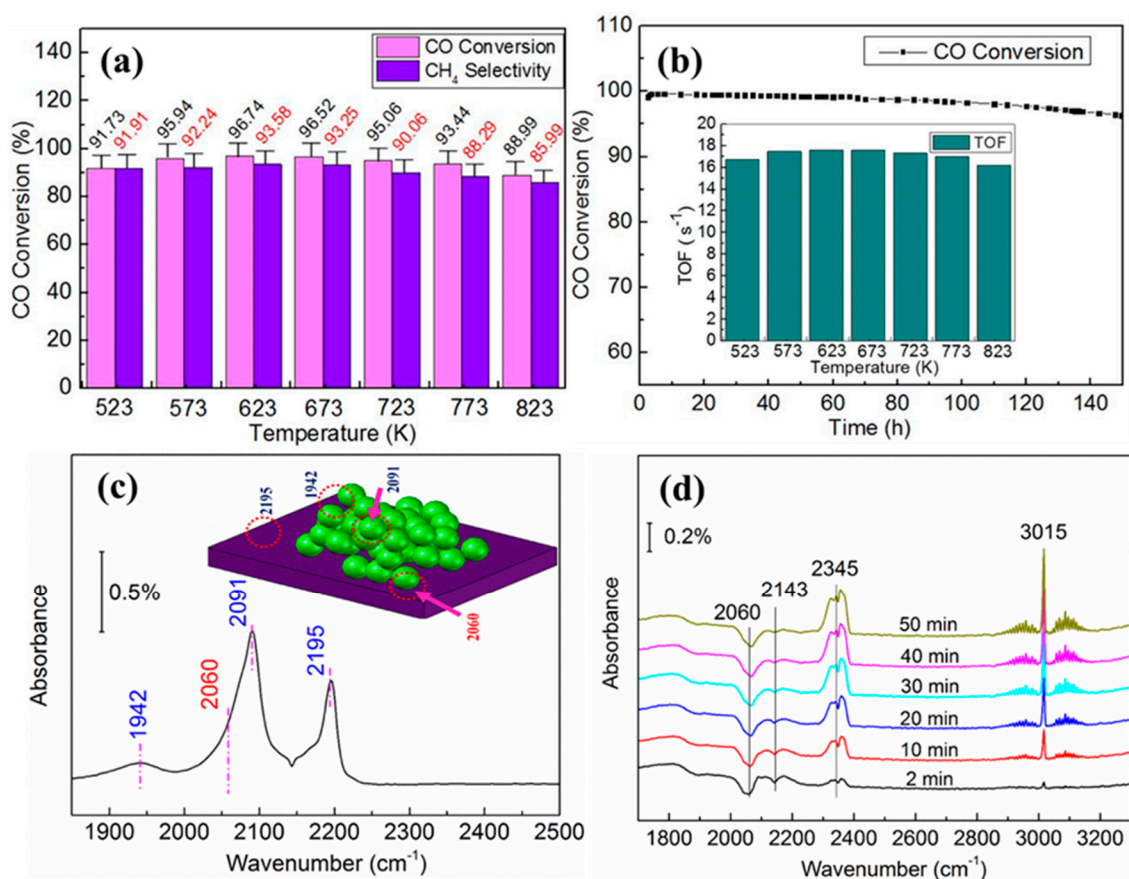


Figure 1. (a) CO conversion and CH₄ selectivity of Ni/SiO₂; (b) turnover frequency (TOF) values and stability at 623 K of Ni/SiO₂. (c) In situ Fourier Transform infrared spectroscopy (FTIR) spectra of Ni/SiO₂ catalyst at 1 mbar CO and room temperature. The reference spectrum was obtained on a clean sample under high vacuum at room temperature. (d) In situ FTIR differential spectra of catalyst Ni/SiO₂ at 500 K in the presence of CO and H₂ at different reaction times. The reference spectrum was the sample spectrum at 1 mbar CO and 500 K. The differential spectrum was recorded immediately after the introduction of 3 mbar H₂ at 500 K.

2.3. Catalyst Characterization

Prior work reported that smaller Ni⁰ particles yield a better catalytic performance, because smaller Ni⁰ particles provide more active sites [12]. Some efforts had been shown to study the active sites on Ni-based catalysts. Agnelli et al. [19] found that the active sites of Ni/SiO₂ comprised one to two adjacent Ni atoms, which were free from adsorbed CO. Liu et al. [20] proposed that defect sites on the metallic Ni⁰ particles dominated the reaction activity. The reaction mechanism on the Ni(111); was studied by experiments and DFT [21,22]. However, the definite active sites in Ni-based catalysts are still unclear.

In order to explore the active sites on Ni/SiO₂ for methanation reactions, in situ vacuum FTIR experiments were used to investigate the CO adsorption behavior on the catalysts. Here, we regarded the in situ FT-IR signals of the samples that were exposed to 1 mbar CO at 500 K as the reference spectrum. The needed differential spectra were obtained by subtracting the reference spectral curve. Four kinds of adsorption sites were selected: the NiO or SiO₂ surface, the top Ni atom surface, the interface between the SiO₂ and Ni atom, and the bridge of the surface Ni atoms [23,24]. Figure 1c shows the in situ IR spectrum of Ni/SiO₂, which was exposed to 1 mbar CO at RT. Three apparent IR bands exist in the spectrum: (a) CO adsorption on the NiO or SiO₂ surface at 2195 cm⁻¹, with a slight blue-shift compared with the gas phase CO; (b) CO adsorption on the top sites of the surface Ni at 2091 cm⁻¹, with a slight red-shift compared with the gas phase CO; (c) CO adsorption on the bridge sites of surface Ni at 1942 cm⁻¹, with a large red-shift compared with the gas phase CO [2]. Two more bands in the spectrum, including the vibration of gaseous CO as indicated by the steep trough centered at 2143 cm⁻¹, and a band at 2060 cm⁻¹, had been overshadowed by other intense bands, such as the asymmetric shape of the band at 2091 cm⁻¹. The exact value of the latter bands could be determined in the following text.

A VTIR spectrum of the CO and H₂ reactions was obtained to explore the catalytic capability of four types of active sites. Four peaks in Figure 1d include a vibration peak with a wave number at 3015 cm⁻¹ from the CH₄ [24], a wave number at 2345 cm⁻¹ from the CO₂ vibration peak [25], then a CO vibration peak with a wave number at 2143 cm⁻¹, and a peak with a wave number at 2060 cm⁻¹ that was ascribed to CO adsorption. The reference spectrum was the sample spectrum under 1 mbar CO at 500 K. Positive peaks in the spectra implied that new species were formed during the process, and negative peaks indicated that the corresponding species were consumed. The in situ transmission infrared spectrum of the CO and H₂ reactions demonstrated that active sites at the interface between SiO₂ and Ni and at 2060 cm⁻¹ were most efficient. With the reaction time increasing, CO was consumed and CH₄ was generated. However, no negative peaks were observed at 2195 cm⁻¹, 2091 cm⁻¹, and 1942 cm⁻¹. The emergence of CO₂ bands indicated that the methanation reaction might exist as a side reaction pathway under the present reaction conditions.

Figure 2a and b show the transmission-electron microscopy (TEM) and high-resolution TEM (HRTEM) images of the Ni/SiO₂ catalyst. On the surface of catalyst, there were a lot of visible black spots, which attributed to Ni particles. Lattice fringes in Figure 2b with a typical d-spacing of 0.282 nm and 0.244 nm were ascribed to the (102) and (112) crystallographic plane of SiO₂ [26,27]. Furthermore, high-angle annular dark field scanning transmission electron microscopy (HAADF-STEM) was used to observe the Ni particles on the surface clearly. Small light spots, which were attributed to small Ni particles, were dispersed uniformly on the catalyst surface (Figure 2c). The detailed particle-size distributions of the Ni/SiO₂ catalyst were determined from the HAADF-STEM image, and the average Ni particle size was 2–3 nm. Figure 2d shows the scanning-electron microscopy (SEM) image of the Ni/SiO₂ catalyst, and the insert shows the Ni mapping. Ni was dispersed uniformly, which agreed well with the HAADF-STEM results. Wide-angle X-ray powder diffraction (XRD) patterns of the Ni/SiO₂ are shown in Figure 2e. The diffraction peak at 21.99° belonged to SiO₂ (JCPDS NO. 77–1316), and the nickel phyllosilicate characteristic peaks (JCPDS NO. 49–1859) were observed at a 2θ of 19.52°, 34.1°, 36.9° and 60.50° [11,28,29]. The peak intensity was weak and exhibited a wide half-peak breadth in the XRD pattern because of the small and finely dispersed of Ni particles [27].

The NiO/SiO₂ catalyst reducibility was characterized by H₂-TPR, as shown in Figure 2f. The TPR profile of NiO/SiO₂ catalyst showed two reduction peaks. The reduction peak centered at 550.8 K resulted from surface NiO reduction [30–32]. Another reduction peak at around 951 K was ascribed to Ni²⁺ ions in bulk phyllosilicates, *i.e.*, NiO species interacted strongly with the support [33–35]. The H₂-TPR profile showed that only some Ni²⁺ was reduced to metal Ni during the pretreatment because of the strong interaction, and thus no Ni diffraction peak was visible in the XRD pattern. Moreover, the results of Ni dispersion by hydrogen adsorption method was detected of 13.7%, which determined a high TOF values and high catalytic performance.

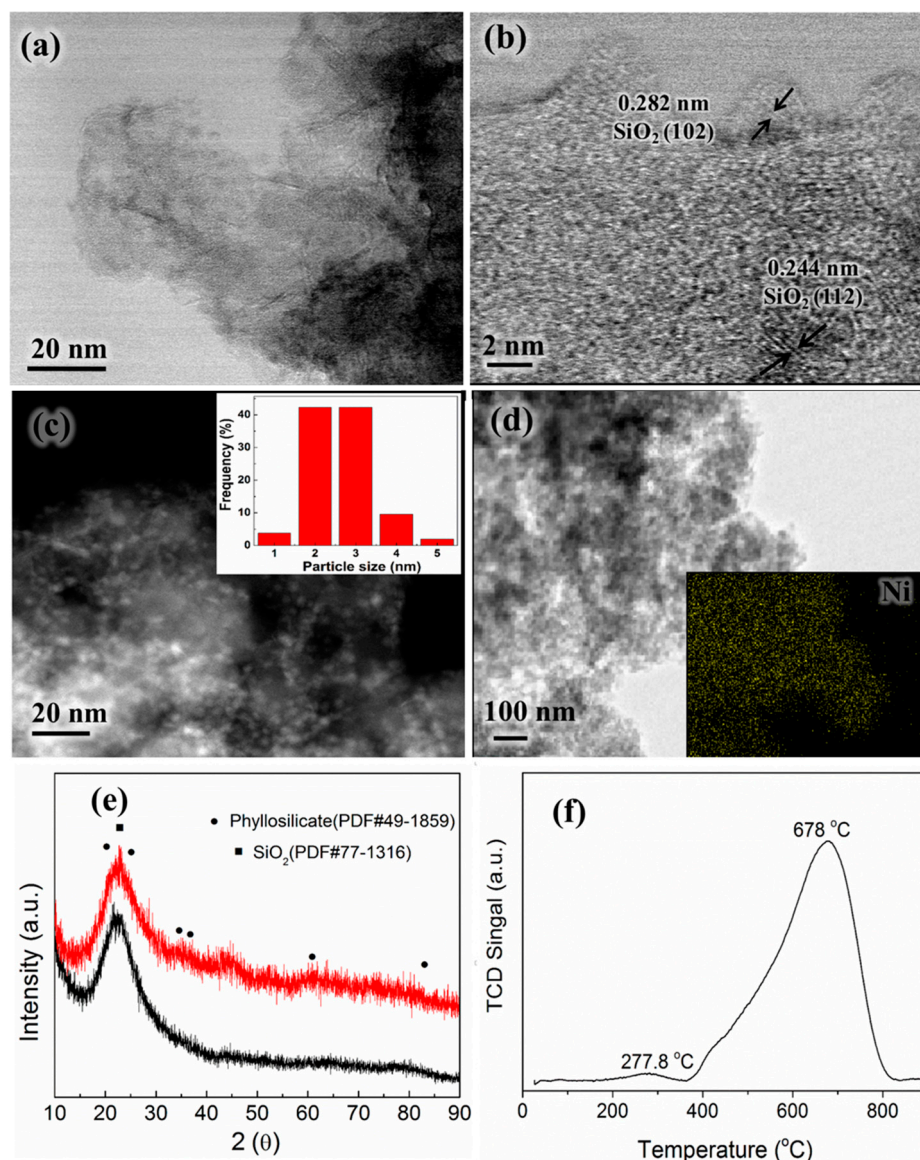


Figure 2. HRTEM (high-resolution transmission-electron microscopy) images of (a,b) Ni/SiO₂, (c) HAADF-STEM (high-angle annular dark field scanning transmission electron microscopy) images and Ni particle-size distribution (inset) for Ni/SiO₂, (d) SEM (scanning-electron microscopy) image of Ni/SiO₂ and Ni mapping (inset), (e) XRD (X-ray powder diffraction) patterns of SiO₂ and Ni/SiO₂, (f) H₂ temperature-programmed reduction (H₂-TPR) of catalyst NiO/SiO₂.

2.4. Various Types of Active Sites

DFT was used to study the CO adsorption behavior in four types of adsorption sites, as shown in Figure 3. Figure 3a shows the CO adsorption models of four different active sites. Figure 3b–e show the calculated IR spectra of four types of CO adsorption models. C–O intramolecular stretching was sensitive on the adsorption sites [36], as described more extensively in original papers [37–40]. The calculated symmetric vibrational modes for CO adsorption at the top Ni atom surface was 1992 cm^{-1} (2131 cm^{-1} after correction), and the experimental value was 2091 cm^{-1} . The calculated symmetric vibrational modes for CO adsorption at the bridge of surface Ni was 1841 cm^{-1} (1980 after correction), with the experimental value of 1942 cm^{-1} .

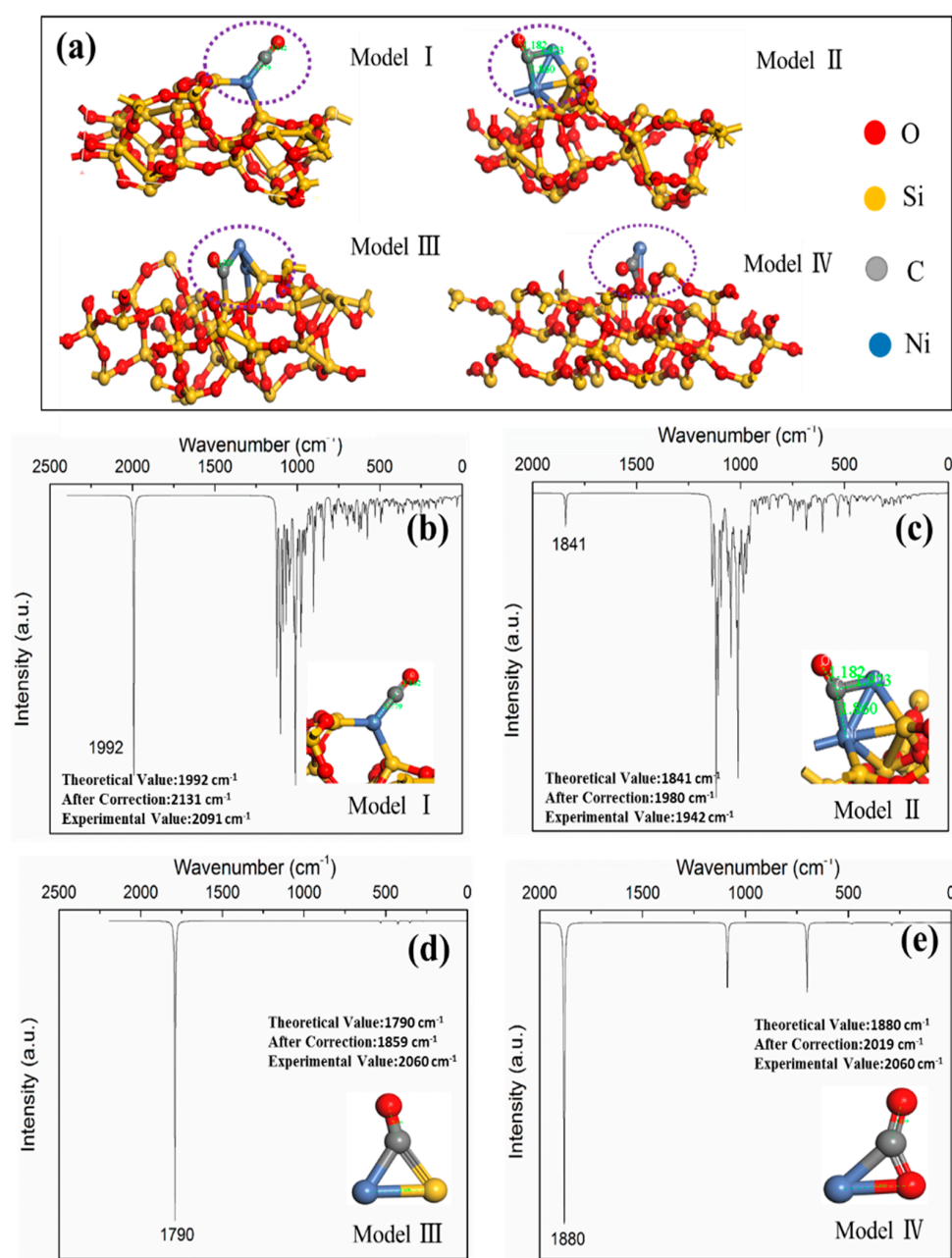


Figure 3. (a) CO adsorption model at different sites. DFT results of (b) SiO₂(111)-modified-CO–Ni-top-spectrum, (c) SiO₂(111)-modified-Ni-bridge-spectrum, (d) Si–Ni-spectrum and (e) O–Ni-spectrum.

There were two situations for CO adsorption at the interface between the Ni and the support SiO₂. (1) CO adsorption between Ni–Si where the theoretical value of the CO symmetric vibrational mode was 1859 cm⁻¹ after correction, and differs by 201 cm⁻¹ compared with the experimental value of 2060 cm⁻¹. (2) CO adsorption between Ni–O where the theoretical value of the CO adsorption was 2019 cm⁻¹ after correction, and the difference between the theoretical and experimental values was 41 cm⁻¹. Because the theoretical value of CO adsorption between Ni–O agreed well with the experimental value, we assume that CO was adsorbed between the Ni–O atoms of the interface between SiO₂ and Ni. And the in situ VTIR spectrum of the CO and H₂ reactions agreed well with previous experimental results, which indicated that with the same Ni content, the smaller Ni particles provided a more support-active ingredient interface and promoted the catalytic performance. Furthermore, with the same size of Ni particles, an increasing Ni loading also could promote catalytic performance. From the experimental results, the as-obtained catalyst with remarkable small Ni particles (2–3 nm) presented more effective active sites, which agreed with the excellent catalytic performance of Ni/SiO₂ catalyst.

3. Materials and Methods

3.1. Ni/SiO₂ Catalyst Preparation

A Ni/SiO₂ catalyst was prepared through the AE method, with the preparation process as follows. A defined amount of Ni(NO₃)₂·6H₂O as the Ni source was dissolved in deionized water to obtain metal precursor solution. Excess of 28% aqueous ammonia solution (analytical-reagent grade, Sinopharm Chemical Reagent Ltd., Shanghai, China) was added to the precursor solution until appeared flocculent material and the quantity was basically constant, and then stirred for 30 min. Afterwards, the requisite quantities of silica sol (Ludox AS-40) was added to the nickel–ammonia-complex solution, where the loading of nickel was 10 wt %. And then, the obtained solution was stirred for another 4 h at 353 K in an oil bath, where the suspension was evaporated. The obtained material was washed with deionized water until there was no pH change (pH = 7) and dried at 353 K for 24 h to obtain catalyst precursors. The catalyst precursors were calcined at 823 K for 4 h in a muffle furnace to produce NiO/SiO₂ catalyst.

3.2. Catalyst Characterization

X-ray diffractometry was used to analyze the crystallographic properties of the materials and XRD patterns were obtained with a BrukerD8 Advance X-ray diffractometer (Bruker Biosciences Corporation, Billerica, MA, USA) with Cu K α radiation in the 2 θ range of 0–90°. H₂-TPR experiments were performed to determine the reducibility of the NiO oxides using a Micromeritics TPx System (Micromeritics ASAP 2720, Micromeritics Instrument Ltd., Norcross, GA, USA) from room temperature to 1173 K at 10 K/min with a 10 vol % H₂/Ar flow of 40 mL/min and by retaining the sample at 1173 K for 20 min. In order to analyze the dispersion of Ni/SiO₂ catalyst, hydrogen adsorption was carried out by Autochem 2920 (Micromeritics Instrument Ltd., Norcross, GA, USA). 0.1 g catalysts were reduced at 750 °C for 1 h in H₂ atmosphere and cooled with N₂ atmosphere. Then H₂ (30 μ L per pulse, carrier gas, N₂ 40 cm³ min⁻¹) was adsorbed by the Ni/SiO₂ catalyst. The catalyst morphology was studied by SEM (Hitachi S-4300 microscope, Hitachi Limited, Japan). TEM and HRTEM images were obtained with a Tecnai F30 field-emission transmission-electron microscope (Hillsboro, OR, USA).

In situ VTIR spectra were recorded by a Thermo Nicolet Is50 spectrometer equipped with a MCT detector cooled by liquid nitrogen and a heating chamber. The catalyst was loaded in a Harrick IR cell and pretreated at 673 K under N₂ at a total flow rate of 100 mL/min for 60 min to remove adsorbed impurities. VTIR spectra were recorded by accumulating 32 scans with a resolution of 4 cm⁻¹. The in situ VTIR spectrometer was constructed from a commercial IR spectrometer (Vertex 70 v, Bruker Corp., Germany). The original measurement compartment was replaced by a stainless-steel chamber that was separated from the IR spectrometer by two KBr windows. An IR beam from the light source in the spectrometer was passed through a sample in the IR chamber and detected

by a deuterated L-alanine-doped triglycine sulfate detector. The base pressure in the spectrometer was better than 0.1 mbar, which can effectively diminish the influence of H₂O and CO₂ during IR measurement. The base pressure in the IR chamber was $\sim 1 \times 10^{-7}$ mbar. A full-range pressure gauge and a capacitance gauge (0.1–1000 mbar) were connected to the chamber to monitor pressure. The Ni/SiO₂ nanoparticles were pressed on a stainless-steel grid (100 mesh, 10 mm × 7 mm) at 20 MPa. The stainless-steel grid with sample was fixed between two molybdenum legs by using two tantalum clamps. Sample heating was achieved by applying a voltage between the two molybdenum legs and electrical current that flowed through the grid heated the sample to 1000 K. A K-type thermocouple was welded carefully on the top center of the grid. In the current configuration, in situ transmission IR measurements can be performed under vacuum and with gas exposure conditions at variable sample temperatures. Before the IR measurement, the Ni/SiO₂ catalyst was annealed at 700 K for 20 min under a high vacuum to ensure that surface contaminations were removed.

3.3. Activity Measurement

The catalytic performance was determined in a fixed-bed reactor. Catalyst (0.156 g) was placed into a tubular reactor and reduced in a H₂ atmosphere for 2 h at 773 K. After cooling to 523 K, synthesis gas (H₂/CO = 3, WHSV = 25,000 mL g⁻¹ h⁻¹) was introduced to the tubular reactor and the pressure was increased to 1.5 MPa. The catalytic performance was evaluated every 50 K between 523–823 K, and the effluent-gas composition was analyzed by online gas chromatography (GC-2014C, SHIMADZU, Kyoto, Japan).

3.4. Density Functional Theory (DFT) Calculations

DFT calculations were performed using a Dmol3 module that was implemented in a DFT electronic structure program [41–43] GGA/PW91 exchange-correlation functional with DND basis set is used to calculate the exchange correlation energy [44]. The self-consistent field (SCF) procedure is used with the tolerance of 10⁻⁶ au and maximum SCF cycles of 500. The calculated vibrational spectra were picked up and analyzed by Dmol3 module (MS8.0, Dassault Systemes Biovia K.K., San Diego, CA, USA, 2014). The calculated vibrational modes of CO adsorbed on Ni/SiO₂ catalyst were corrected by the standard gas CO spectra.

4. Conclusions

A Ni/SiO₂ catalyst was successfully prepared by the AE method. The Ni/SiO₂ catalyst displayed an excellent catalytic performance over the reaction temperature range with a 96.7% CO conversion and 95.6% CH₄ selectivity at 623 K, and 9.5 s⁻¹ TOF at 523 K, 1.5 MPa and a WHSV of 25,000 mL·g⁻¹·h⁻¹. The catalyst exhibited an excellent thermostability over 150 h at 623 K. The in situ VTIR and DFT results demonstrated that the catalysts highly dispersed active sites at the interfaces between the support and active component were responsible for their high catalytic efficiencies. The decrease in particle size of the active component to a single atom may provide excellent catalytic performance. We, therefore, believe that the clarification of active sites provides a strategy to design and prepare high-efficiency CO methanation catalysts.

Author Contributions: F.Y., H.Q. and H.G. designed and administered the experiments. M.Z., P.L. performed experiments. Z.T., J.L., M.Z., W.F. and B.D. collected and analyzed data. All authors discussed the data and wrote the manuscript.

Acknowledgments: This work was financially supported by National Natural Science Foundation of China (U1203293), High-end Talent Team Construction Foundation (No. 108-10000318), Program for Changjiang Scholars and Innovative Research Team in University (No. IRT_15R46) and Program of Science and Technology Innovation Team in Bingtuan (No. 2015BD003).

Conflicts of Interest: The authors declare no conflicts of interests.

References

1. Kamata, H.; Tian, Z.Q.; Izumi, Y.; Choong, C.K.S.; Chang, J.; Schreyer, M.; Chen, L.; Borgna, A. Dispersed and high loading Ni catalyst stabilized in porous SiO₂ matrix for substituted natural gas production. *Catal. Today* **2018**, *299*, 193–200. [[CrossRef](#)]
2. Konishcheva, M.V.; Potemkin, D.I.; Snytnikov, P.V.; Stonkus, O.A.; Belyaev, V.D.; Sobyenin, V.A. The insights into chlorine doping effect on performance of ceria supported nickel catalysts for selective CO methanation. *Appl. Catal. B Environ.* **2018**, *221*, 413–421. [[CrossRef](#)]
3. Wind, T.L.; Falsig, H.; Sehested, J.; Moses, P.G.; Nguyen, T.T.M. Comparison of mechanistic understanding and experiments for CO methanation over nickel. *J. Catal.* **2016**, *342*, 105–116. [[CrossRef](#)]
4. Li, P.; Yu, F.; Altaf, N.; Zhu, M.; Li, J.; Dai, B.; Wang, Q. Two-Dimensional Layered Double Hydroxides for Reactions of Methanation and Methane Reforming in C1 Chemistry. *Materials* **2018**, *11*, 221. [[CrossRef](#)] [[PubMed](#)]
5. Wang, H.; Xu, K.; Yao, X.; Ye, D.; Pei, Y.; Hu, H.; Qiao, M.; Li, Z.H.; Zhang, X.; Zong, B. Undercoordinated Site-Abundant and Tensile-Strained Nickel for Low-Temperature CO_x Methanation. *ACS Catal.* **2018**, *1207–1211*. [[CrossRef](#)]
6. Lv, Y.; Xin, Z.; Meng, X.; Tao, M.; Bian, Z. Ni based catalyst supported on KIT-6 silica for CO methanation: Confinement effect of three dimensional channel on NiO and Ni particles. *Micropor. Mesopor. Mater.* **2018**, *262*, 89–97. [[CrossRef](#)]
7. Vita, A.; Italiano, C.; Pino, L.; Frontera, P.; Ferraro, M.; Antonucci, V. Activity and stability of powder and monolith-coated Ni/GDC catalysts for CO₂ methanation. *Appl. Catal. B Environ.* **2018**, *226*, 384–395. [[CrossRef](#)]
8. Zhao, B.; Chen, Z.; Chen, Y.; Ma, X. Syngas methanation over Ni/SiO₂ catalyst prepared by ammonia-assisted impregnation. *Int. J. Hydrogen Energy* **2017**, *42*, 27073–27083. [[CrossRef](#)]
9. Lai, Y.Q.; Wang, Q.Y.; Wang, M.R.; Li, J.; Fang, J.; Zhang, Z.A. Facile synthesis of mesoporous Fe–N–C electrocatalyst for high performance alkaline aluminum-air battery. *J. Electroanal. Chem.* **2017**, *801*, 72–76. [[CrossRef](#)]
10. Yan, X.; Liu, Y.; Zhao, B.; Wang, Z.; Wang, Y.; Liu, C.-J. Methanation over Ni/SiO₂: Effect of the catalyst preparation methodologies. *Int. J. Hydrogen Energy* **2013**, *38*, 2283–2291. [[CrossRef](#)]
11. Zhao, B.; Chen, Z.; Yan, X.; Ma, X.; Hao, Q. CO Methanation over Ni/SiO₂ Catalyst Prepared by Ammonia Impregnation and Plasma Decomposition. *Top. Catal.* **2017**, *60*, 879–889. [[CrossRef](#)]
12. Li, P.; Zhu, M.; Dan, J.; Kang, L.; Lai, L.; Cai, X.; Zhang, J.; Yu, F.; Tian, Z.; Dai, B. Two-dimensional porous SiO₂ nanomesh supported high dispersed Ni nanoparticles for CO methanation. *Chem. Eng. J.* **2017**, *326*, 774–780. [[CrossRef](#)]
13. Yao, Y.; Goodman, D.W. In situ IR spectroscopic studies of Ni surface segregation induced by CO adsorption on Cu-Ni/SiO₂ bimetallic catalysts. *Phy. Chem. Chem. Phys.* **2014**, *16*, 3823–3829. [[CrossRef](#)] [[PubMed](#)]
14. Loc, L.C.; Huan, N.M.; Gaidai, N.A.; Thoang, H.S.; Nekrasov, N.V.; Agafonov, Y.A.; Lapidus, A.L. Reaction mechanism of CO methanation on nickel catalysts, as studied by isotopic and nonstationary methods. *Kinet. Catal.* **2011**, *52*, 749–755. [[CrossRef](#)]
15. Martra, G.; Swaan, H.M.; Mirodatos, C.; Kermarec, M.; Louis, C. Sintering of Ni/SiO₂ catalysts prepared by impregnation and deposition-precipitation during CO hydrogenation. *Stud. Surf. Sci. Catal.* **1997**, *111*, 617–624.
16. Primet, M.; Dalmon, J.A.; Martin, G.A. Adsorption of CO on well-defined Ni/SiO₂ catalysts in the 195–373 K range studied by infrared spectroscopy and magnetic methods. *J. Catal.* **1977**, *46*, 25–36. [[CrossRef](#)]
17. Gao, J.; Jia, C.; Zhang, M.; Gu, F.; Xu, G.; Su, F. Effect of nickel nanoparticle size in Ni/ α -Al₂O₃ on CO methanation reaction for the production of synthetic natural gas. *Catal. Sci. Technol.* **2013**, *3*, 2009–2015. [[CrossRef](#)]
18. Feng, J.-T.; Lin, Y.-J.; Evans, D.G.; Duan, X.; Li, D.-Q. Enhanced metal dispersion and hydrodechlorination properties of a Ni/Al₂O₃ catalyst derived from layered double hydroxides. *J. Catal.* **2009**, *266*, 351–358. [[CrossRef](#)]
19. Agnelli, M.; Swaan, H.M.; Marquez-Alvarez, C.; Martin, G.A.; Mirodatos, C. CO Hydrogenation on a Nickel Catalyst: II. A Mechanistic Study by Transient Kinetics and Infrared Spectroscopy. *J. Catal.* **1998**, *175*, 117–128. [[CrossRef](#)]

20. Liu, B.; Yao, N.; Li, S.; Wang, J.; Lv, D.; Li, X. Methanation of CO in hydrogen-rich gas on Ni–Ru/SiO₂ catalyst: The type of active sites and Ni–Ru synergistic effect. *Chem. Eng. J.* **2016**, *304*, 476–484. [[CrossRef](#)]
21. Zhi, C.; Wang, Q.; Wang, B.; Li, D.; Zhang, R. Insight into the mechanism of methane synthesis from syngas on a Ni(111) surface: a theoretical study. *RSC Adv.* **2015**, *5*, 66742–66756. [[CrossRef](#)]
22. Han, X.; Yang, J.; Guo, H.; Qin, Z.; Zhao, S.; Lu, Y.; Li, Z.; Ren, J. Mechanism studies concerning carbon deposition effect of CO methanation on Ni-based catalyst through DFT and TPSR methods. *Int. J. Hydrogen Energy* **2016**, *41*, 8401–8411. [[CrossRef](#)]
23. Layman, K.A.; Bussell, M.E. Infrared Spectroscopic Investigation of CO Adsorption on Silica-Supported Nickel Phosphide Catalysts. *J. Phy. Chem. B* **2004**, *108*, 10930–10941. [[CrossRef](#)]
24. Konishcheva, M.V.; Potemkin, D.I.; Badmaev, S.D.; Snytnikov, P.V.; Paukshtis, E.A.; Sobyenin, V.A.; Parmon, V.N. On the Mechanism of CO and CO₂ Methanation Over Ni/CeO₂ Catalysts. *Top. Catal.* **2016**, *59*, 1424–1430. [[CrossRef](#)]
25. Westermann, A.; Azambre, B.; Bacariza, M.C.; Graça, I.; Ribeiro, M.F.; Lopes, J.M.; Henriques, C. Insight into CO₂ methanation mechanism over NiUSY zeolites: An operando IR study. *Appl. Catal. B Environ.* **2015**, *174–175*, 120–125.
26. Zhu, X.; Cheng, D.; Kuai, P. Catalytic Decomposition of Methane over Ni/Al₂O₃ Catalysts: Effect of Plasma Treatment on Carbon Formation. *Energy Fuels* **2008**, *22*, 1480–1484. [[CrossRef](#)]
27. Zhang, C.; Yue, H.; Huang, Z.; Li, S.; Wu, G.; Ma, X.; Gong, J. Hydrogen Production via Steam Reforming of Ethanol on Phyllosilicate-Derived Ni/SiO₂: Enhanced Metal–Support Interaction and Catalytic Stability. *ACS Sustain.Chem. Eng.* **2013**, *1*, 161–173. [[CrossRef](#)]
28. Zhang, Q.; Wang, M.; Zhang, T.; Wang, Y.; Tang, X.; Ning, P. A stable Ni/SBA-15 catalyst prepared by the ammonia evaporation method for dry reforming of methane. *RSC Adv.* **2015**, *5*, 94016–94024. [[CrossRef](#)]
29. Dėbek, R.; Motak, M.; Galvez, M.E.; Grzybek, T.; Da Costa, P. Promotion effect of zirconia on Mg(Ni,Al)O mixed oxides derived from hydrotalcites in CO₂ methane reforming. *Appl. Catal. B Environ.* **2018**, *223*, 36–46. [[CrossRef](#)]
30. Kadirvelu, K.; Thamaraiselvi, K.; Namasivayam, C. Removal of heavy metals from industrial wastewaters by adsorption onto activated carbon prepared from an agricultural solid waste. *Bioresour. Technol.* **2001**, *76*, 63–65. [[CrossRef](#)]
31. Lakshmanan, P.; Kim, M.S.; Park, E.D. A highly loaded Ni@SiO₂ core–shell catalyst for CO methanation. *Appl. Catal. A Gen.* **2016**, *513*, 98–105. [[CrossRef](#)]
32. Damyanova, S.; Pawelec, B.; Palcheva, R.; Karakirova, Y.; Sanchez, M.C.C.; Tyuliev, G.; Gaigneaux, E.; Fierro, J.L.G. Structure and surface properties of ceria-modified Ni-based catalysts for hydrogen production. *Appl. Catal. B Environ.* **2018**, *225*, 340–353. [[CrossRef](#)]
33. Sun, K.-Q.; Marceau, E.; Che, M. Evolution of nickel speciation during preparation of Ni-SiO₂ catalysts: effect of the number of chelating ligands in [Ni(en)_x(H₂O)_{6-2x}]²⁺ precursor complexes. *Phy. Chem. Chem. Phy.* **2006**, *8*, 1731–1738. [[CrossRef](#)] [[PubMed](#)]
34. Li, P.; Wen, B.; Yu, F.; Zhu, M.; Guo, X.; Han, Y.; Kang, L.; Huang, X.; Dan, J.; Ouyang, F.; et al. High efficient nickel/vermiculite catalyst prepared via microwave irradiation-assisted synthesis for carbon monoxide methanation. *Fuel* **2016**, *171*, 263–269. [[CrossRef](#)]
35. Le, T.A.; Kim, M.S.; Lee, S.H.; Kim, T.W.; Park, E.D. CO and CO₂ methanation over supported Ni catalysts. *Catal. Today* **2017**, *293–294*, 89–96.
36. Politano, A.; Chiarello, G. Vibrational Investigation of Catalyst Surfaces: Change of the Adsorption Site of CO Molecules upon Coadsorption. *J. Phy. Chem. C* **2011**, *2*, 514–517. [[CrossRef](#)]
37. Politano, A.; Chiarello, G. Carbon monoxide interaction with oxygenated nickel single-crystal surfaces studied by vibrational spectroscopy. *Vib. Spectrosc.* **2011**, *55*, 295–299. [[CrossRef](#)]
38. Politano, A.; Chiarello, G. The formation of HOCO in the coadsorption of water and carbon monoxide on Pt₃Ni(111). *RSC Adv.* **2014**, *4*, 45641–45646. [[CrossRef](#)]
39. Chiarello, G.; Marino, A.R.; Formoso, V.; Politano, A. The adsorption and co-adsorption of oxygen and carbon monoxide on Pt₃Ni(111): A vibrational study. *J. Chem. Phy.* **2011**, *134*, 224705. [[CrossRef](#)] [[PubMed](#)]
40. Politano, A.; Vitiello, M.S.; Viti, L.; Hu, J.; Mao, Z.; Wei, J.; Chiarello, G. Unusually strong lateral interaction in the CO overlayer in phosphorene-based systems. *Nano Res.* **2016**, *9*, 2598–2605. [[CrossRef](#)]
41. Delley, B. An all-electron numerical method for solving the local density functional for polyatomic molecules. *J. Chem. Phy.* **1990**, *92*, 508–517. [[CrossRef](#)]

42. Delley, B. From molecules to solids with the DMol3 approach. *J. Chem. Phys.* **2000**, *113*, 7756–7764. [[CrossRef](#)]
43. Gao, H. A first principles investigation of the NO oxidation mechanism on Pt/ γ -Al₂O₃. *RSC Adv.* **2016**, *6*, 102914–102923. [[CrossRef](#)]
44. Perdew, J. P.; Wang, Y. Accurate and simple analytic representation of the electron-gas correlation energy. *Phys. Rev. B* **1992**, *45*, 13244–13249. [[CrossRef](#)]



© 2018 by the authors. Licensee MDPI, Basel, Switzerland. This article is an open access article distributed under the terms and conditions of the Creative Commons Attribution (CC BY) license (<http://creativecommons.org/licenses/by/4.0/>).